THE JOURNAL OF BIOLOGICAL CHEMISTRY VOL. 283, NO. 19, pp. 13459–13470, May 9, 2008
Printed in the U.S.A.

Effect of the Active Site D25N Mutation on the Structure, Stability, and Ligand Binding of the Mature HIV-1 Protease*[S]

Received for publication, October 12, 2007, and in revised form, January 11, 2008 Published, JBC Papers in Press, February 15, 2008, DOI 10.1074/jbc.M708506200

Jane M. Sayer[‡], Fengling Liu[§], Rieko Ishima[¶], Irene T. Weber[§], and John M. Louis[‡1]

From the [‡]Laboratory of Chemical Physics, NIDDK, National Institutes of Health, Bethesda, Maryland 20892-0520, the [§]Department of Biology, Georgia State University, Atlanta, Georgia 30303, and the [¶]Department of Structural Biology, School of Medicine, University of Pittsburgh, Pittsburgh, Pennsylvania 15260

All aspartic proteases, including retroviral proteases, share the triplet DTG critical for the active site geometry and catalytic function. These residues interact closely in the active, dimeric structure of HIV-1 protease (PR). We have systematically assessed the effect of the D25N mutation on the structure and stability of the mature PR monomer and dimer. The D25N mutation (PR_{D25N}) increases the equilibrium dimer dissociation constant by a factor >100-fold (1.3 ± 0.09 μM) relative to PR. In the absence of inhibitor, NMR studies reveal clear structural differences between PR and PR_{D25N} in the relatively mobile P1 loop (residues 79–83) and flap regions, and differential scanning calorimetric analyses show that the mutation lowers the stabilities of both the monomer and dimer folds by 5 and 7.3 °C, respectively. Only minimal differences are observed in high resolution crystal structures of PR_{D25N} complexed to darunavir (DRV), a potent clinical inhibitor, or a non-hydrolyzable substrate analogue, Ac-Thr-Ile-Nle-r-Nle-Gln-Arg-NH_2 (RPB), as compared with PR·DRV and PR·RPB complexes. Although complexation with RPB stabilizes both dimers, the effect on their T_m is smaller for PR_{D25N} (6.2 °C) than for PR (8.7 °C). The T_m of PR_{D25N}·DRV increases by only 3 °C relative to free PR_{D25N}, as compared with a 22 °C increase for PR·DRV, and the mutation increases the ligand dissociation constant of PR_{D25N}·DRV by a factor of ~10^6 relative to PR·DRV. These results suggest that interactions mediated by the catalytic Asp residues make a major contribution to the tight binding of DRV to PR.

In HIV-1,[2] the protease is synthesized as part of a 165-kDa polyprotein (Gag-Pol). Gag-Pol comprises the matrix, capsid, P2, nucleocapsid, transframe, protease (PR), reverse transcriptase, and integrase domains (1). The protease mediates its own release and the processing of the viral polyproteins, Gag and Gag-Pol, into the necessary structural and functional proteins (1–3). This spatio-temporally regulated process is crucial for the maturation and propagation of HIV (4–7). Because of this vital role, the mature protease dimer has proven to be a successful target for the development of antiviral agents. Structure-based design of drugs targeted against the mature protease has aided in the development of potent inhibitors that bind specifically to the active site (8, 9). Although several of these inhibitors are in clinical use and have curtailed the progression of the disease, the effectiveness of long term treatment has been limited due to naturally selected protease variants exhibiting lower affinity to the drugs than the wild-type enzyme, and this has been a challenge for the past decade (10). In recent years, a major emphasis in protease research has been to improve inhibitor design and treatment regimens, which include the highly active retroviral therapy, to overcome the problem of drug resistance and curb progress of the disease (11, 12).

The HIV-1 protease is composed of 99 amino acids and is a member of the family of aspartic acid proteases (1, 13). Unlike the cellular aspartic proteases that are active as monomers, catalytic activity of retroviral proteases, including HIV-1 protease, requires dimer formation (14). The active site is formed along the dimer interface, and each subunit contributes one of the two catalytic aspartic acid residues (1, 14). These residues are expected to be in opposite states of protonation for activity, and the water molecule involved in the hydrolysis of the peptide bond is proposed to be hydrogen bonded to the aspartyl residues (15, 16). Hydrolysis of the peptide bond mediated by the protease involves general base/general acid catalysis. The importance of the Asp-25 residue for protease function was confirmed in studies showing that it is required for catalytic activity and viral infectivity (2). Subsequent studies showed that coexpression of the wild-type proviral DNA with increasing amounts of the mutant proviral DNA bearing the D25N mutation results in a concomitant decrease in the proteolytic activity

* This work was authored, in whole or in part, by National Institutes of Health staff. This work was supported, in whole or in part, by the Intramural Research Program of the NIDDK, National Institutes of Health (NIH), and NIH Grant GM62920. This work was also supported by the Molecular Basis of Disease Program, the Georgia Research Alliance, and the Georgia Cancer Coalition. The costs of publication of this article were defrayed in part by the payment of page charges. This article must therefore be hereby marked "*advertisement*" in accordance with 18 U.S.C. Section 1734 solely to indicate this fact.

The atomic coordinates and structure factors (codes 3BVA and 3BVB) have been deposited in the Protein Data Bank, Research Collaboratory for Structural Bioinformatics, Rutgers University, New Brunswick, NJ (http://www.rcsb.org/).

[S] The on-line version of this article (available at http://www.jbc.org) contains supplemental Figs. S1–S4 and Table S1.

[1] To whom correspondence should be addressed: Laboratory of Chemical Physics, NIDDK, NIH, Bldg. 5, Rm. B2-29, Bethesda, MD 20892-0520. Tel.: 301-594-3122; Fax: 301-480-4001; E-mail: johnl@intra.niddk.nih.gov.

[2] The abbreviations used are: HIV-1, human immunodeficiency virus type 1; PR, mature HIV-1 protease; r.m.s.d., root mean square deviation; Nle, norleucine; DRV, darunavir; RPB, Ac-Thr-Ile-Nle-r-Nle-Gln-Arg-NH_2 non-hydrolyzable substrate analogue inhibitor with a reduced peptide bond indicated by r (carbonyl replaced by CH_2); substrate IV, Lys-Ala-Arg-Val-Nle-(4-nitrophenylalanine)-Glu-Ala-Nle-NH_2; ITC, isothermal titration calorimetry; DSC, differential scanning calorimetry; TFR, transframe region consisting of the N-terminal transframe octapeptide followed by the 48-amino acid $p6^{pol}$. The notation used for equilibrium constants is as follows: K_d, dimer dissociation constants of dimeric protease constructs; K_a, binding (association) constants for ligands with dimeric protease constructs; K_L, ligand dissociation constants defined as $1/K_a$.

monitored by *in vivo* viral polyprotein processing (17). This suggested that the protease domain bearing the D25N mutation is capable of adopting a native-like fold to sequester the wild-type protease via heterodimer formation. Because the protease bearing this mutation is completely devoid of catalytic activity, it is a useful tool for studies of the protease under conditions where the active protease tends to undergo rapid autoproteolysis (self-degradation). Additionally, the inactivating mutation D25N makes it possible to investigate the binding of substrates to the protease without the interference of the accompanying proteolytic cleavage reaction. Thus, the mature protease and its precursor bearing the D25N mutation have been effectively used in such studies with substrates corresponding to the natural cleavage sites in the Gag and Gag-Pol polyproteins by x-ray crystallography and NMR (10, 18).

The steps in the maturation of the Gag-Pol precursor and the mechanism of the autocatalytic maturation of the protease have been studied extensively (3, 10). Upon its intramolecular maturation at its N terminus, the protease forms a stable dimer concomitant with the formation of the terminal β-sheet structure and a very low equilibrium dimer dissociation constant ($K_d < 10$ nM) (10). It is predicted that disrupting the terminal β-sheet arrangement of the mature protease, which contributes to ~50% of the total dimer interface contacts, or preventing dimer formation prior to its maturation may provide an alternative avenue for inhibitor design (10, 11, 19, 20). This presumably non-competitive mode of inhibition might show a synergistic effect to the conventional active site targeted compounds with the advantage of reducing the emergence of drug-resistant strains. Several groups have reported the development of dimerization inhibitors of the mature protease; however, none of these kinds of potential lead compounds have been characterized further for possible clinical use (19). Recent complementary NMR structural and biophysical studies of the mature protease and its precursor have aimed to elucidate the role of conserved regions required for a native-like fold, dimer formation, and precursor maturation. Several subtle mutations have been identified that increase the K_d by ~2 to >5 orders of magnitude, thus also enabling the solution structure determination of the protease monomer by NMR (10). It is anticipated that insights derived from such studies will aid in the discovery and rational design of novel inhibitors of dimerization.

In our exploration of sites that are critical for dimer formation, we had observed that a D25N mutation also significantly increases the K_d (21). In the present study we report the characterization of the effects of this mutation on the dimer stability, inhibitor/substrate binding, and the molecular structure and dynamics of the protease by a multifaceted approach comprising NMR, calorimetry, and crystallography.

EXPERIMENTAL PROCEDURES

Vector Construction and Protein Preparation—The pseudo wild type (PR) (22) and the active site mutant (PR_{D25N}) mature protease constructs were expressed using pET11a vector and *Escherichia coli* BL21(DE3) host, purified from inclusion bodies and folded from a denatured state as described (22, 23). The expression and purification of PR_{T26A}, $PR_{D25N/T26A}$, and $^{SFNF}PR_{D25N}$ constructs has been described previously (24). A new construct, $PR_{5-95/D25N}$, was generated using the PR_{5-95} DNA template (23), appropriate forward and reverse primers, and the QuikChange protocol (Stratagene). The newly introduced mutation was verified both by DNA sequencing and mass spectrometry. To maintain consistency in the analysis, all constructs bear five mutations, Q7K, L33I and L63I (which restrict the autoproteolysis (self-degradation) of active proteases), and C67A and C97A, to prevent cysteine thiol oxidation (22). They differ only in their specified mutations (shown in subscripts). Proteins for NMR studies were obtained by growing the cells in minimal media containing [^{15}N]ammonium chloride with or without [^{13}C]glucose as the sole nitrogen and carbon sources, respectively.

Inhibitors and Substrate—The non-hydrolyzable substrate analog inhibitor RPB, Ac-Thr-Ile-Nle-r-Nle-Gln-Arg-NH_2, in which r (reduced peptide bond) represents a methylene group that replaces the peptide carbonyl, was obtained from Bachem Bioscience Inc. (King of Prussia, PA). Darunavir (DRV) was a generous gift of Dr. Arun Ghosh, Purdue University, and was subsequently obtained from the National Institutes of Health (NIH) AIDS research and reference reagent program, Division of AIDS, NIAID, NIH: Reagent 11447 from Tibotec Pharmaceuticals. Substrate IV, Lys-Ala-Arg-Val-Nle-(4-nitrophenyl-alanine)-Glu-Ala-Nle-NH_2, was purchased from California Peptide Research (Napa, CA).

NMR Experiments—All NMR data were recorded on DMX500 spectrometers with or without a cryoprobe (Bruker Instruments, Billerica, MA) at 20 °C. ^{1}H-^{15}N correlation spectra of PR_{D25N} were acquired using ^{15}N-labeled protein at 0.5 mM in 20 mM phosphate buffer at pH 5.8 and 25 μM in 50 mM acetate buffer at pH 5.0. Backbone chemical shifts were assigned based on HNCA type experiments using a 0.5 mM ^{15}N,^{13}C-labeled protein at pH 5.8, similar to those used to assign chemical shifts of PR previously (25). Experiments to determine transverse relaxation time, T_2, and ^{15}N-{^{1}H} NOE values were carried out using 0.5 mM ^{15}N-labeled protein at pH 5.8 as described previously (26).

Isothermal Titration Calorimetry—Measurements were performed using a high precision VP-ITC titration calorimetric system (MicroCal Inc.) at 28 °C. PR and PR_{D25N} were prepared according to the quench protocol of protein folding (23) to a final concentration of 6.9 μM and 14.7 μM, respectively, by mixing 1 volume of protein in 30–50 mM formic acid with 2.3–2.5 volumes of 5 mM sodium acetate, pH 6, and then with 3.3–4 volumes of 100 mM sodium acetate, pH 5 (buffer mix). The RPB inhibitor was dissolved in the same buffer mix to a final concentration of 300 μM. For titration of PR_{D25N} with DRV, the buffered PR_{D25N} solution contained a final protein concentration of 11 μM. The DRV solution was prepared at a final concentration of 266 μM and contained a final concentration of 0.5% Me_2SO derived from the DRV stock solution. Me_2SO was added to the enzyme solution to give the same 0.5% concentration, to eliminate possible thermal effects on dilution of the organic solvent from the titrant. Analyses of the data were performed using Origin software provided with the instrument.

Differential Scanning Calorimetry—Measurements were performed using a VP-DSC microcalorimeter (MicroCal Inc.). Samples were prepared by the quench protocol (23) as above to

give a final protein concentration of 26–33 μM as monomer and a buffer concentration of 50 mM sodium acetate at pH 4.8. Thermal denaturation scans were begun at a temperature of 20 or 25 °C and run at a rate of 90 °C/h, except for $^{SFNF}PR_{D25N}$ (60 °C/h). The final temperature ranged from 85 to 100 °C depending on the observed T_m. Raw data from representative DSC scans of each of the protease constructs are given in supporting information (supplemental Fig. S1). Reversibility as determined by assaying PR (22) before and after scanning showed an ~90% loss of activity after one scan. In the experiments with RPB and DRV inhibitors, the inhibitor was present at a final concentration of 30 μM (approximately twice the concentration of the dimeric proteins). For the DSC of PR_{D25N} with substrate IV, the final substrate concentration was 360 μM. Reference (buffer) scans were subtracted from the observed traces, and the data were normalized for protein (monomer or dimer) concentration. Linear baseline segments were selected in regions of the trace before and after the transition peak, and the Origin software of the instrument was then used to generate and subtract a "progress baseline" between them that reflects the fraction of the total reaction completed at each temperature point (as described in the MicroCal data analysis manual). The apparent T_m was determined from the resultant peak maximum. Because of the lack of reversibility, rigorous thermodynamic analysis was not possible, and no attempt was made to determine ΔC_p or ΔH for the transitions.

Crystallographic Analysis—Crystals were grown at 20–25 °C by vapor diffusion using the hanging drop method. Mutant PR_{D25N} was co-crystallized with the potent clinical inhibitor, DRV, in a protein to inhibitor molar ratio of 1:2. The reservoir contained 0.2 M sodium acetate buffer, pH 5.0, and 30% sodium chloride as precipitant. PR_{D25N} was co-crystallized with RPB in a molar ratio of 1:20 in the reservoir containing 0.1 M citrate/0.2 M phosphate buffer, pH 5.4, 10% sodium chloride as precipitant, and 5–10% Me_2SO. The protein (1.8–3.5 mg/ml) was preincubated on ice. The crystallization drops had a 1:1 ratio by volume of reservoir solution and protein. The crystals grew in 1–7 days and were frozen in liquid nitrogen with a cryoprotectant of 20–30% glycerol.

X-ray diffraction data for both complexes were collected on the SER-CAT beamline of the Advanced Photon Source, Argonne National Laboratory. Data were processed using HKL2000 (27). The structures were solved by molecular replacement using AmoRe (28), refined using SHELX (29) and refitted using O (30). Alternate conformations were modeled for residues when obvious in the electron density maps. The solvent was modeled with over 100 water molecules, and ions present in the crystallization solutions, as described previously (31). Anisotropic B factors were refined for all the structures. Hydrogen atom positions were included in the last stage of refinement using all data once all other parameters, including disorder, had been modeled. The structures have been submitted to the Protein Data Bank with accession code 3BVB for PR_{D25N}·DRV and 3BVA for PR_{D25N}·RPB.

RESULTS AND DISCUSSION

Monomer-Dimer Equilibria—Because PR_{D25N} is not catalytically active, it was not possible to measure its K_d by analysis of the dependence of enzymatic activity on protein concentration as in the case of PR (22). We have previously observed differences in the ^1H-^{15}N HSQC spectra of protease constructs that exist predominantly as dimers or as monomers and assigned the signals characteristic of each species (32). Hence this method was used to characterize the monomer-dimer equilibrium of PR_{D25N}. At ~0.5 mM concentration in 20 mM sodium phosphate, pH 5.8, 20 °C, we observed a ^1H-^{15}N HSQC spectrum for PR_{D25N} (Fig. 1*A*) in the absence of bound inhibitor that is similar to that observed for PR (32), indicating that it is essentially dimeric at this concentration. We have recently described a simple protocol (see quench protocol in Ref. 23) for preparing folded dimers and monomeric mutants of the protease at low concentrations of ~20 μM, suitable for NMR and other biophysical studies. Under these conditions (an ~20-fold lower protein concentration than in Fig. 1*A*), signals corresponding to a minor fraction become more evident in the PR_{D25N} spectrum (Fig. 1*B*). Although the signals of the minor component were not assigned due to overlap with the dimer signals, it is apparent from comparing the previously assigned chemical shifts of PR_{R87K} and PR_{1-95} monomers (24, 32) that the minor fraction observed in Fig. 1*B* corresponds to the PR_{D25N} monomer. On the basis of the signal intensities of the characteristic monomer peaks and the corresponding dimer peaks, the K_d of the PR_{D25N} dimer was determined to be 1.3 ± 0.09 μM, at pH 5.0. These values are similar to those previously determined qualitatively for PR_{D25N} by NMR (21) and by sedimentation equilibrium analysis at pH 7.0 (33), and approximately two orders of magnitude larger than the value of ~0.01 μM previously estimated for PR from kinetic data (22). Thus, in addition to suppression of catalytic activity, the D25N mutation significantly affects the monomer-dimer equilibrium of the mature protease.

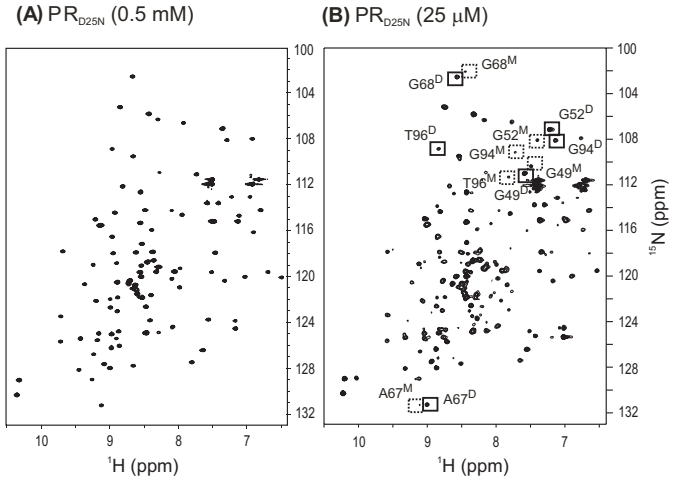

FIGURE 1. **^1H-^{15}N HSQC spectra of PR_{D25N} at 0. 5 mM (*A*) and 25 μM (*B*) protein concentrations.** Proteins were prepared and folded as described previously (23). Peaks unique to the dimer and the monomer are shown in *solid* and *dashed boxes*, respectively.

Effects on Thermal Stability—In earlier studies we had shown that the quench protocol of preparing folded protease permitted NMR and fluorescence measurements under similar conditions. Under the conditions described (23), folded protease samples can be prepared easily prior to each experiment from

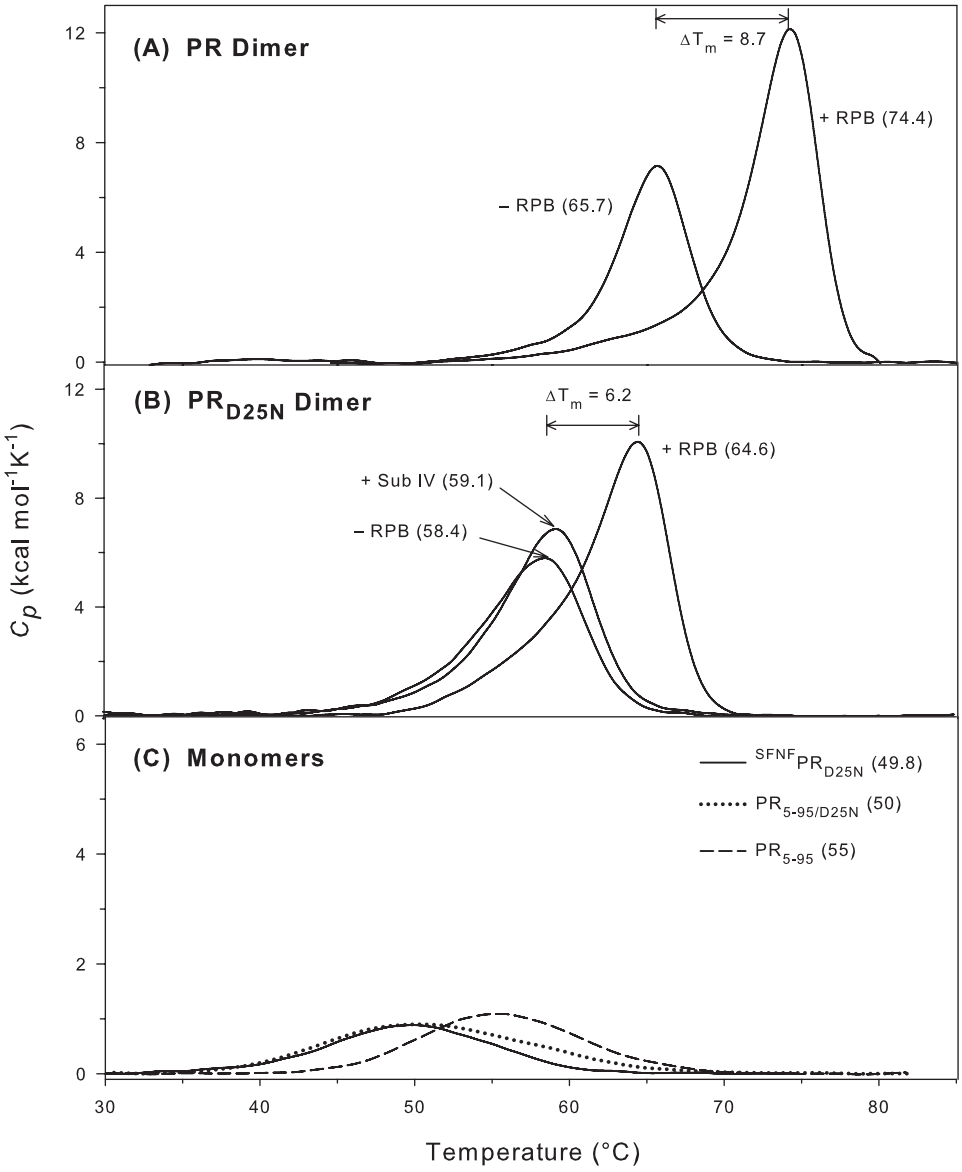

FIGURE 2. **DSC thermograms of dimer and monomer constructs.** For conditions see "Experimental Procedures." The *numbers* correspond to the apparent T_m of each protein (maximum of the transition) in °C. Data shown are baseline-corrected and normalized to the appropriate dimer or monomer concentrations. *A*, dimeric PR (13 μM) in the presence and absence of 30 μM of RPB inhibitor; *B*, dimeric PR_{D25N} (14.5 μM) in the presence and absence of 30 μM RPB and of 360 μM substrate IV (*Sub IV*); *C*, monomeric PR_{5-95} (32 μM), $^{SFNF}PR_{D25N}$ (25 μM) and monomeric $PR_{5-95/D25N}$ (33 μM). Note that the mass of protein per unit volume is approximately the same in *C* as in *A* and *B*, although the molarity of the monomers is double the molarity of the dimers; the *ordinate scale* of *C* is expanded for comparability with *A* and *B*.

the same stock solutions maintained in an unfolded state, usually in 30–50 mM formic acid. This has enabled the facile preparation and comparison of the thermal stabilities of PR, PR_{D25N}, and several related constructs (supporting information, supplemental Table S1). Consistent with the difference in dimer stability, the D25N mutation results in a significant (7.3 °C) decrease in the T_m determined from the peak maxima of the transitions for unfolding/dimer dissociation relative to PR as measured by DSC at pH 4.8 (Fig. 2, *A* and *B*). Previous observations that the midpoints of urea denaturation curves for PR (22) and PR_{D25N} (23) both occur at ~2 M urea had indicated no significant difference between PR_{D25N} and PR. The present observations may result from mechanistic differences between the thermal and urea denaturation processes of the protease. Constructs that lack the terminal residues 1–4 and 96–99 critical for the dimer interface exist as folded monomers in solution (23). Thus, we examined the effect of the D25N mutation on monomer stability by comparing the thermal stabilities of PR_{5-95} and $PR_{5-95/D25N}$. The T_m for $PR_{5-95/D25N}$ is 5 °C lower than for PR_{5-95} (Fig. 2*C*). These observations indicate that Asp-25 plays a significant role in stabilizing the monomer and dimer folds and is consistent with the greater sensitivity to urea denaturation of $PR_{D25N/T26A}$ (midpoint of the denaturation curve at ~1.8 M urea) relative to PR_{T26A} (midpoint at ~2.5 M urea), both of which are folded monomers (23).

The native transframe region (TFR) flanking the N terminus of the protease comprises two domains, the conserved transframe octapeptide followed by the 48 amino acid $p6^{pol}$, both separated by a protease cleavage site (see Fig. 1 in Ref. 23). It appears that the monomer-dimer equilibrium of the protease is modulated by the N-terminally flanking TFR, such that prior to the cleavage at the $p6^{pol}$/PR junction, the protease domain is mainly monomeric ($K_d > 0.5$ mM), exhibiting a fold that is similar to that of a single subunit of the dimer at least for the region spanning residues 10–90 (24). Residues 1–9 and 91–99 display no specific structure (24). These studies were facilitated using the precursor construct TFR-PR bearing a D25N mutation to abolish autoprocessing (24). Subsequently it was found that a four-residue extension at the N terminus of the protease (Ser-Phe-Asn-Phe corresponding to the C-terminal residues of $p6^{pol}$) increased the K_d of the resulting construct $^{SFNF}PR_{D25N}$ by more than three orders of magnitude (24). Because the full-length TFR portion of the larger fusion protein may possess some intrinsic structure (34) that could interfere with interpretation of the DSC results, we utilized the same $^{SFNF}PR_{D25N}$ construct to investigate whether the presence of the SFNF sequence affects only the magnitude of K_d or whether it also alters the stability of the monomer fold. In fact, the DSC thermograms for $^{SFNF}PR_{D25N}$ and $PR_{5-95/D25N}$ monomers were found to be nearly superimposable, and their T_m values are the same within experimental error (Fig. 2*C*). The identical T_m values for the

monomer fold in the presence and absence of the SFNF modification supports the conclusion that this N-terminal tetrapeptide influences only the stability of the dimer. This is consistent with the interpretation (23) that the SFNF sequence may inhibit dimerization via interactions with protease residues 3–6 at the dimer interface, a region that does not contribute to the monomer structure.

The thermal stabilities of PR and PR_{D25N} were also determined in the presence of a substrate-analogue inhibitor with a reduced peptide bond (RPB, see "Experimental Procedures" and Fig. 6*B*). Repetitive scanning indicated that the thermal transition was irreversible under these conditions. Little or no change in the heat capacity before and after the transition was apparent, possibly as a result of this irreversibility. Because the observed process was not reversible, detailed thermodynamic analysis was not possible. In the presence of 30 μM RPB, ~two times the PR dimer concentration and at least 100 times the ligand dissociation constant (K_L) for PR·RPB (see following section), the T_m values for both PR (Fig. 2*A*) and PR_{D25N} (Fig. 2*B*) are significantly increased (by 8.7 and 6.2 °C, respectively). This qualitatively indicates that RPB binding to the active site stabilizes both proteins, although the relative stabilization is larger with PR. In light of this observation it was important to determine quantitatively the extent to which the structural factors that influence the monomer-dimer equilibrium also affect the interactions of the mutant protein with substrates and inhibitors.

Although the affinity of PR for RPB has been measured by kinetic inhibition studies (22), this approach cannot be used to determine an analogous binding constant for the catalytically inactive protein PR_{D25N}. Thus, ITC of PR_{D25N} with RPB under conditions similar to those employed for the inhibition studies was used to determine K_L. Fig. 3 shows the titration of PR (*A*) and PR_{D25N} (*B*) with 300 μM RPB inhibitor at 28 °C in 50 mM sodium acetate buffer, pH 5. Curve fitting of the integrated data (Table 1) gave binding constants (K_a) of $(1.86 \pm 0.76) \times 10^7$ and $(3.30 \pm 0.56) \times 10^6$ M^{-1}, corresponding to $K_L = 1/K_a$ values of ~0.05 and ~0.3 μM, for PR·RPB and PR_{D25N}·RPB, respectively. The affinity of PR_{D25N} for RPB falls within the ideal range for ITC (Fig. 3*B*) and permitted accurate determination of K_L for this construct. Although the higher affinity of PR for RPB resulted in a much steeper titration curve with fewer data points in the transition region (Fig. 3*A*), the value of K_L ~0.05 μM for PR·RPB, while subject to greater experimental uncertainty, was reasonably consistent with the value previously determined by kinetics (22) under similar conditions. Thus the substitution of Asn for Asp at the active site of the protease decreases the affinity of the enzyme for RPB by a factor of ~6.

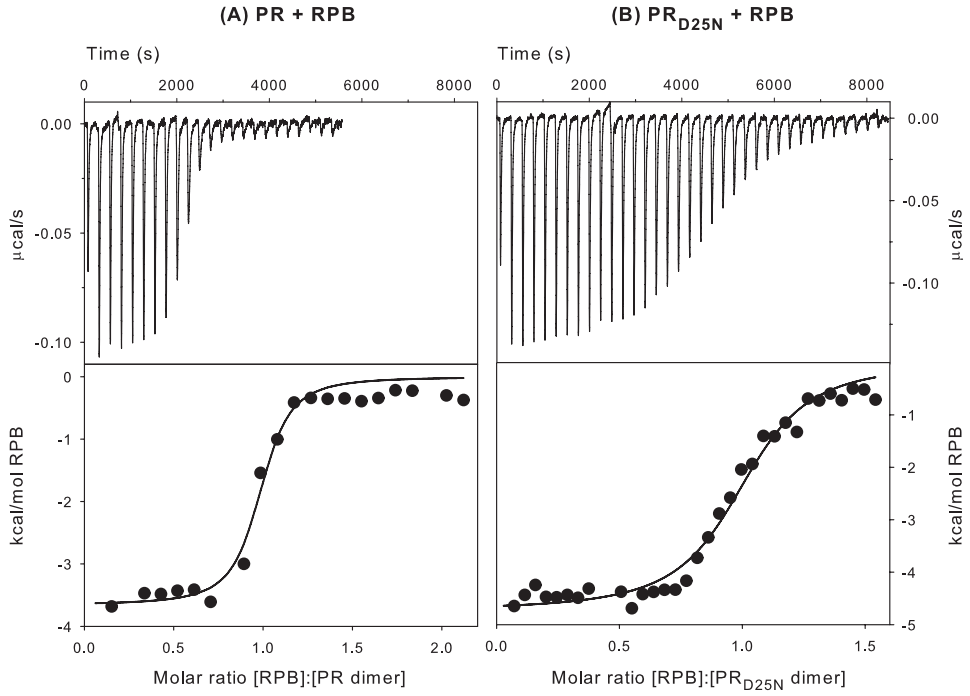

FIGURE 3. **ITC of PR (*A*) and PR_{D25N} (*B*) with RPB inhibitor in 50 mM sodium acetate buffer, pH 5, at 28 °C.** *A*, thermal changes on addition of 3-μl aliquots of 300 μM RPB inhibitor to PR or PR_{D25N} (6.9 and 14.7 μM, respectively) in the calorimetric cell (~1.43 ml).) Curve fitting of the integrated data (*lower panels*) gave values of the dissociation constants ($K_L = 1/K_a$; see Table 1) of ~0.05 and ~0.3 μM for PR·RPB and PR_{D25N}·RPB, respectively.

Interestingly, the enthalpies (ΔH) of RPB binding to PR and PR_{D25N} are comparable (Table 1), whereas the entropy (ΔS) is considerably smaller for binding of RPB to PR_{D25N} than to PR. At 28 °C, approximately two-thirds of the binding energy for PR·RPB derives from $T\Delta S$, whereas the enthalpic and entropic contributions are similar for PR_{D25N}·RPB. Although part of the favorable entropy for formation of both complexes derives from desolvation of the inhibitor, the *difference* in entropy between the two systems with a common inhibitor must reflect changes in properties of the proteins upon binding to RPB. This may result in part from differences in the flap mobility of the two

TABLE 1
Fitted ITC data for PR and PR_{D25N} binding to ligands in sodium acetate buffer at pH 5

Protease construct	Ligand	Binding constant (K_a)	ΔH	ΔS	Stoichiometry
		M^{-1}	*cal/mol*	*cal/mol*	[*ligand*]/[*protein*]
PR	RPB	$(1.86 \pm 0.76) \times 10^7$	−3,661 ± 114	21.1	0.95 ± 0.02
	DRV[a]	2.2×10^{11}	−12,100	10.5	
PR_{D25N}	RPB	$(3.30 \pm 0.56) \times 10^6$	−4,738 ± 87	14.1	1.00 ± 0.01
	DRV	$(3.17 \pm 0.29) \times 10^5$	−5,812 ± 206	5.9	1.03 ± 0.03

[a] For wild-type PR in 10 mM sodium acetate buffer, pH 5, at 20 °C (data from Ref. 38).

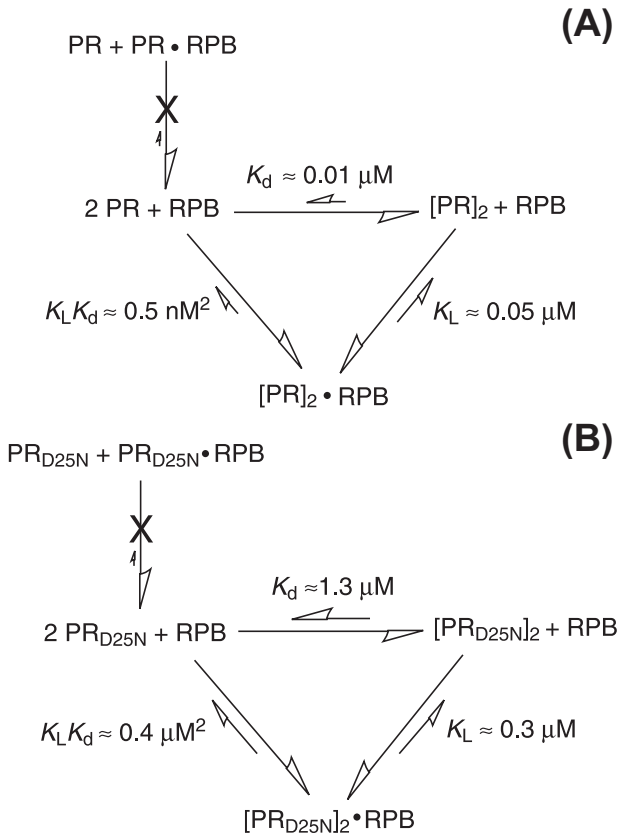

FIGURE 4. **Thermodynamic cycles showing the relationship between the equilibrium constants ($K_L K_d$) for unfolding/dissociation of dimeric PR·RPB (*A*) and PR_{D25N}·RPB (*B*) complexes, the equilibrium constants (K_L) for dissociation of RPB from the dimers, and the equilibrium constants (K_d) for dissociation of the uncomplexed dimers.** Binding of the inhibitor to monomeric PR or PR_{D25N} is expected to be insignificant; thus the equilibria are shown as proceeding exclusively via inhibitor binding to the dimers. The values of K_L shown for RPB inhibitor were determined by ITC (present work). K_d values were determined from kinetic data (23) and NMR spectral analysis (present work, Fig. 1) for PR and PR_{D25N}, respectively. *PR* in this scheme denotes the monomer.

unliganded proteins as suggested by the NMR data below. The negative ΔS for constraining the more-mobile PR_{D25N} flaps on binding RPB may be larger than for PR, with a net effect of decreasing the overall positive ΔS.

As noted above, destabilization caused by the D25N mutation results in a lowering of the T_m for unfolding/dimer dissociation by 7.3 °C (see Fig. 2, *A* and *B*). In the presence of 30 μM RPB, this lowering of the T_m is even larger (9.8 °C), because it results from *both* the lower affinity of PR_{D25N} for RPB and its decreased dimer stability. Combination of the equilibrium constants for inhibitor dissociation from the dimer (K_L) and for dimer dissociation to monomers (K_d), according to the thermodynamic cycle depicted in Fig. 4, gives an overall equilibrium constant for dissociation of the RPB-dimer complex that is ~800-fold greater for PR_{D25N} relative to PR (note micromolar *versus* nanomolar scale), whereas, in the absence of RPB, the equilibrium constant for dissociation of the PR_{D25N} dimer is ~100-fold greater relative to PR. The difference between ΔT_m in the presence and absence of RPB for PR (8.7 °C) relative to the analogous ΔT_m for PR_{D25N} (6.2 °C) is clearly related to the 8- to 10-fold difference in affinity of the inhibitor for the two proteins.

Although we observed substantial effects of the D25N mutation on both the dimer stability of the protease and its ability to bind RPB, there is less of an effect on binding of a less tightly bound substrate. K_L for substrate IV, a chromogenic analogue of the CA-p2 cleavage site in the Gag polyprotein, bound to PR_{D25N} had previously been determined by NMR to be ~270 μM (21). ITC titration of 14.5 μM PR_{D25N} (as dimer) with 1.4 mM substrate IV under the above conditions was performed to try to confirm the magnitude of this value. Although this K_L was too large (corresponding to weak binding) to permit determination by ITC, the curvature observed in a plot of the integrated thermal response (kcal/mol) *versus* molar ratio (0–13 mol of substrate/mol of protein) (data not shown) was consistent with the value measured by NMR. A control titration in the absence of protein showed a constant thermal response for each successive addition of substrate over the entire range of the titration. Further evidence for weak binding of substrate IV was obtained from a DSC scan of PR_{D25N} in the presence of 360 μM substrate IV, in the concentration range used for PR enzyme assays (22). The T_m for PR_{D25N} was virtually unaffected by the presence of this substrate ($\Delta T_m < 1$ °C; *cf.* Fig. 2*B*). The binding affinities of PR_{D25N} ($K_L \sim 270\ \mu$M from NMR, see above) and PR ($K_m = 177\ \mu$M) (22) for substrate IV differ by a factor of less than two, in comparison with the ~6-fold difference in binding affinity of these two proteins for RPB. We suggest that this difference may relate to the tighter binding of the RPB inhibitor, which "freezes" both proteins into a similar conformation (see crystal structures) at some energetic cost to the mutated relative to the native protein, whereas the more loosely bound substrate gives a more flexible enzyme·substrate complex, which can better accommodate small structural differences between the proteins.

The K_d for PR has been determined from the dependence on enzyme concentration of the hydrolysis rate of substrate IV (22, 35). This method involves a potential ambiguity in that the substrate could stabilize the dimer, resulting in an observed K_d value that is smaller than the actual value for the unbound enzyme. Although it is not possible to measure the T_m for enzymatically active PR in the presence of substrate IV, which would be rapidly cleaved, our present observation that assay concentrations of this substrate contribute minimally to the stabilization of PR_{D25N} suggests that this substrate would also not significantly stabilize the PR dimer under the same conditions and supports the conclusion that the kinetically measured K_d correctly represents the dimer dissociation constant for the unbound PR dimer.

Crystal Structures of PR_{D25N} in Complex with Inhibitors: Comparison with PR—In light of the sizable effects of the D25N mutation on the monomer/dimer equilibrium and inhibitor binding, crystallography was used to attempt to identify a structural basis for the dimer destabilization as well as for the less effective binding of the RPB inhibitor by PR_{D25N} relative to PR. The crystal structures of PR_{D25N} complexed with DRV and RPB were determined and compared with the corresponding complexes (PDB accession codes 2IEN and 2AOD, respectively) of PR. The crystallographic statistics are listed in Table 2. The crystal structures of PR_{D25N}·DRV and PR_{D25N}·RPB were refined to an *R*-factor of 0.15 at the resolution of 1.3 Å and 0.14 at the resolution

of 1.05 Å, respectively. Both crystal structures have one dimer in the asymmetric unit of space group $P2_12_12$. The inhibitor DRV is bound in the active site cavity of PR_{D25N} in two orientations with relative occupancies of 74%/26%, whereas the RPB inhibitor shows only one orientation in its complex with PR_{D25N}, as had previously been observed with PR (36). Side-chain disorder was observed at P1 (Nle) and P4 (Arg) of RPB, which are flexible residues and frequently disordered in other crystal structures (36, 37). Electron density maps of DRV and RPB are provided in the supporting information (supplemental Fig. S2).

Alternate conformations were modeled for some side-chain atoms of the protein, *e.g.* residues 7, 41, 65, and 70 in one or both subunits. The *B*-factors of those residues were normally higher than for other residues that were smaller or had interactions with other residues. The Ile-50 at the tip of the flap had alternate conformations of the main-chain and side-chain atoms in PR_{D25N}·DRV but not in PR_{D25N}·RPB. Water molecules (140–195) and other solvent species, including sodium ions, chloride ions, and glycerol molecules, were modeled to fit in the electron density maps.

Overall, the conformations of PR_{D25N} in complex with these two inhibitors, whose affinities for PR differ by >3 orders of magnitude, DRV (K_L for PR ~5 pM (38)) and RPB (K_L for PR ~30 nM, this work), are very similar to the corresponding enzyme·inhibitor complexes of PR (Fig. 5). Upon superimposition of the crystal structures, the r.m.s.d. of all Cα atoms between PR·DRV and PR_{D25N}·DRV was 0.14 Å, and between PR·RPB and PR_{D25N}·RPB, it was only 0.09 Å. However, the r.m.s.d. is only an indicator of macroscopic differences in the structure and folding of the protein. In general, the overall structures of HIV-1 protease constructs are very similar even when they contain mutated residues and/or different bound small molecules, although large local structural differences have been observed in some cases. For example, in PR_{F53L}, Ile-50 at the tips of the flaps was shifted up to 2.5 Å, although the main-chain r.m.s.d. was only 0.4 Å (39). Some structural differences may also arise from crystal packing. Thus, the r.m.s.d. of main chain or Cα structures of PR is usually <0.6 Å for structures with different space groups and cell units, and <0.3 Å for structures in the same space groups and cell units (31, 37, 40). In the present structures of PR_{D25N}, not only the overall chain conformation but also the positions of critical amino acid side chains are in most cases strikingly similar to those observed in the corresponding PR structures. In the present study we focus on two specific regions of the protease that are essential for its structural integrity and catalytic activity, namely, the dimer interface and the active site.

TABLE 2
Crystallographic data statistics

Protease construct	PR_{D25N}	PR_{D25N}
Inhibitor	DRV	RPB
Space group	$P2_12_12$	$P2_12_12$
Unit cell dimensions (Å)		
a	58.3	58.0
b	85.9	85.8
c	46.1	46.5
Unique reflections	51,872	102,685
R_{merge} (%)	6.2	13.6
All data (final shell)	(62.1)	(35.4)
I/σ (I)	17.5	22.3
All data (final shell)	(2.2)	(2.7)
Resolution range for refinement (Å)	10–1.30	10–1.05
R_{work} (%)	15.0	14.3
R_{free} (%)	19.7	17.1
No. of waters	143	195
Completeness (%)	89.8	94.6
All data (final shell)	(71.8)	(82.1)
r.m.s.d. from ideality		
Bonds (Å)	0.013	0.017
Angle distance (Å)	0.033	0.040
Average *B*-factors (Å^2)		
Main chain	18.5	10.3
Side chain	25.9	16.9
Inhibitor	22.2	14.1
Solvent	31.0	27.3

The Dimer Interface—The dimer of PR is maintained by interactions between the two subunits, including the terminal residues (1–4 and 96–99), the tips of the flaps (50 and 51), Asp-29, Arg-87, and Arg-8′ (3, 10, and 20), and residues in and surrounding the active site (residues 24–27) (41). Some relatively small differences between PR and PR_{D25N} were observed in these regions. In the terminal region, the ring of Pro-1 is bent away from the ring of Phe-99′ in both PR_{D25N}·DRV and PR_{D25N}·RPB complexes. The atom CG of Pro-1 is shifted by 0.8 Å away from Phe-99′ in one subunit and 0.5 Å in the other subunit in PR_{D25N}·DRV (see supplemental Fig. S3*A*), whereas the shifts are 0.5 Å and 0.3 Å, respectively, in PR_{D25N}·RPB (not shown). Thus, some CH . . . π interactions stabilizing the two subunits at the termini appear to be weaker in the PR_{D25N} mutant. The distance between NH_2 and OD2 of Arg-8 and Asp-29′ is 0.3 Å longer in PR_{D25N}·DRV than in PR (see supplemental Fig. S3*B*). However, this contact is identical (2.8 Å) in the PR_{D25N} and PR complexes with RPB (not shown). In general, these interactions in the dimer interface are somewhat less tight in PR_{D25N} than in PR, which is consistent with the increased value of K_d for PR_{D25N}. Notably, however, there are virtually no differences in the crucial "fireman's grip" region at the bottom of the active site cavity. Specifically, the inter-oxygen distances between the hydroxyl oxygen of Thr-26 and the carbonyl of Leu-24, which form a hydrogen bond that is critical for dimerization (41), are virtually identical (2.7 Å). Small

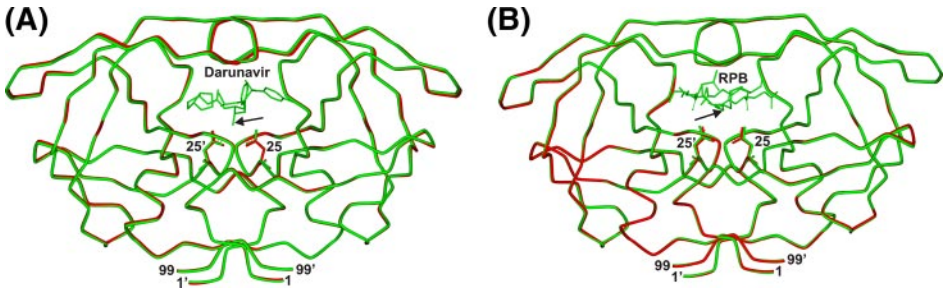

FIGURE 5. **Comparison of the crystal structures of PR (*red*)- and PR_{D25N} (*green*)-inhibitor complexes.** Tube representations of PR bound to DRV (*A*) or RPB (*B*) superimposed on PR_{D25N} bound to DRV (*A*) or RPB (*B*) ranging from 1.05- to 1.4-Å resolution. Inhibitors, DRV and RPB, and the active site residue 25 are shown as *stick models*, and the terminal residues are indicated. The location of a central motif consisting of a hydroxyl group in DRV that can hydrogen bond to the catalytic Asp-25 is indicated by the *black arrow*.

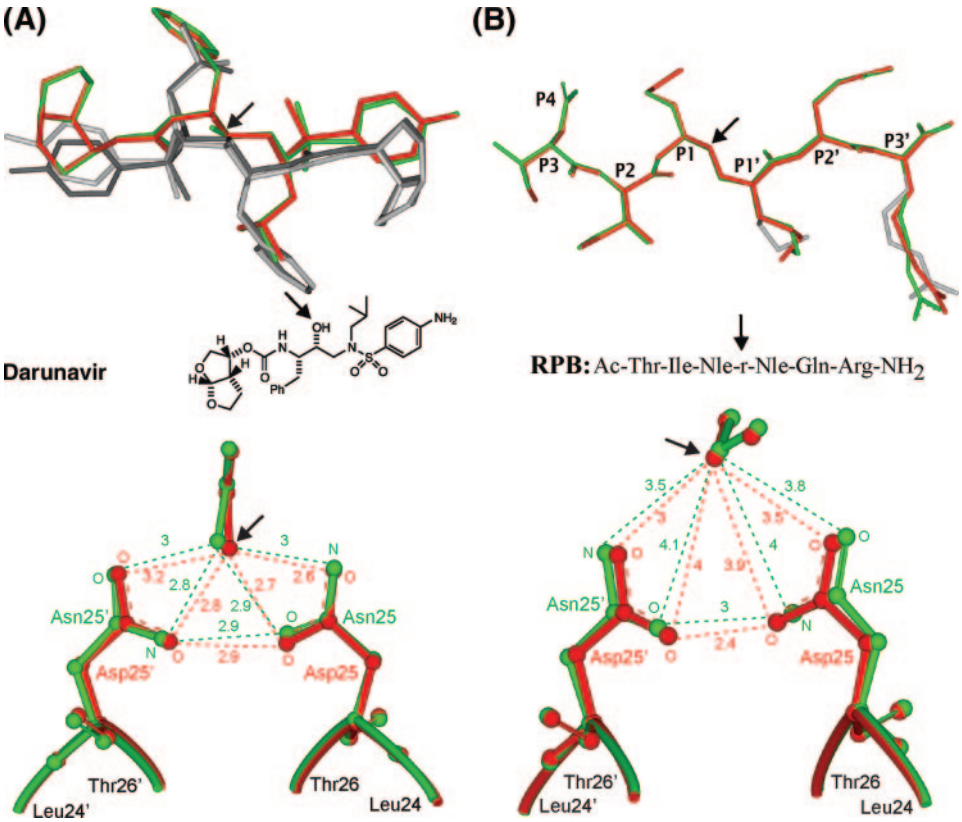

FIGURE 6. **Comparison of the inhibitor structures bound to either PR (*red* or *black*) or PR_{D25N} (*green* or *gray*).** DRV binding (*A*) was observed in two orientations with relative occupancies of 55% (*red*) to 45% (*black*) in PR·DRV (2IEN (32)) and 76% (*green*) to 24% (*gray*) in PR_{D25N}·DRV. RPB binding (*B*) was observed in a single orientation (*red* in PR (2AOD (37)) or *green* in PR_{D25N}). Distances between the active site residues and the inhibitor (*black arrows*) are indicated in angstroms. Residues P4–P3′ of the RPB inhibitor are marked, and alternate conformations of P1′ and P3′ side chains are indicated in *gray*.

differences in the orientations of the catalytic Asp-25/Asn-25 residues are discussed in the following section.

Interactions with Inhibitors at the Active Site—The inhibitor DRV is bound in the active site cavity of PR_{D25N} in a major (74% occupancy) and a minor (26% occupancy) orientation (Fig. 6*A*). The same orientations were observed in the complex with PR, with a nearly equal distribution of the two populations (55%/45% (31)). For a given orientation, the conformation of DRV is similar in both the PR and PR_{D25N} complexes (Fig. 6*A*), except for differences in the position of the aniline ring in the minor orientation. Detailed structures are shown in supplemental Fig. S4. Generally, the distances between atoms of DRV and residues of PR are similar or 0.2–0.4 Å longer in PR_{D25N} than in PR. In the major orientation, the distance between aniline N1 of DRV and the peptide O atom of Asp-30 is 3.3 Å in PR_{D25N}, whereas the equivalent distance is 2.9 Å in PR. In addition, the distance between aniline C4 and CH3 of Ile-84 in PR_{D25N}·DRV is 0.3 Å longer than in PR·DRV. Some larger structural differences are observed in the minor orientation of DRV. The terminal aniline rings in the minor orientation do not align well on superimposition of the PR and PR_{D25N} structures, such that their N1 atoms are displaced by 1.2 Å relative to each other (Fig. 6*A* and supplemental Fig. S4*B*). By comparison, this displacement is only 0.2 Å for the major orientation (supplemental Fig. S4*A*). The shift of the aniline ring causes changes in the interactions between this ring in the minor orientation and its neighboring residues of PR. A H-bond (3.2 Å) between aniline N1 and the peptide O atom of Asp-30′ in the complex PR·DRV is absent in PR_{D25N}·DRV. However, the separation of N1 and the delta O of Asp-30′ is 2.5 Å compared with 2.9 Å in the PR complex. This is one of the few shorter distances in PR_{D25N} than in PR. Also the distance between aniline C4 and CH3 of Ile-84′ in PR_{D25N} is 0.8 Å longer than in PR.

In complexes with both DRV and RPB, the geometry of the catalytic Asp pair is perturbed very little on substitution by Asn. For the protein·RPB complexes, examination of the Asn-25 and Asn-25′ pair of PR_{D25N} superimposed on the corresponding Asp pair of PR indicates a difference in position of only 0.3–0.5 Å between corresponding O and N atoms (Fig. 6*B*); in the DRV complexes (Fig. 6*A*), this difference is even smaller: 0.2–0.3 Å. The distances between RPB and the two catalytic aspartic acids in PR_{D25N} are 0.1–0.3 Å longer than in PR. The distance between two adjacent O atoms of Asp-25 and Asp-25′ is 2.4 Å in PR·RPB, and the corresponding distance between atom OD1 of Asn-25 and ND2 of Asn-25′ is 3.0 Å in PR_{D25N}·RPB (Fig. 6*B*). This 0.6-Å increase in the distance between the closest atoms of Asp/Asn-25 and 25′ in PR_{D25N}·RPB relative to PR·RPB is consistent with the lowered thermal stability of the mutant dimer·RPB complex. However, the equivalent distances for PR·DRV and PR_{D25N}·DRV are identical (2.9 Å, Fig. 6*A*). Although the differences are small, the structural comparison of PR and PR_{D25N} indicates that DRV has weaker overall interactions with PR_{D25N} than with PR (see calorimetric results below).

Unlike DRV, the RPB inhibitor exhibits only one orientation when bound to PRand PR_{D25N} (Fig. 6*B*). The conformations of RPB complexed with PR and PR_{D25N} are very similar on superimposition of the structures, as are the Asp and Asn-25 residues. This indicates that the 6-fold reduced affinity of RPB for PR_{D25N} relative to PR cannot be explained by steric effects alone, and is likely related to the destabilization of the fold induced by the mutation. The PR_{D25N}·RPB complex ($K_L \sim 0.3$ mM) appears to exhibit a slightly better "fit" and fewer structural perturbations than the PR_{D25N}·DRV complex ($K_L = 3.2$ mM) on superimposition with the corresponding structures containing PR, consistent with the lower binding affinity of DRV with PR_{D25N} (see below).

Structure and Dynamics of Free PR_{D25N} in Solution—Earlier results have indicated that the active, mature protease crystallizes rather readily only in complex with an inhibitor or non-

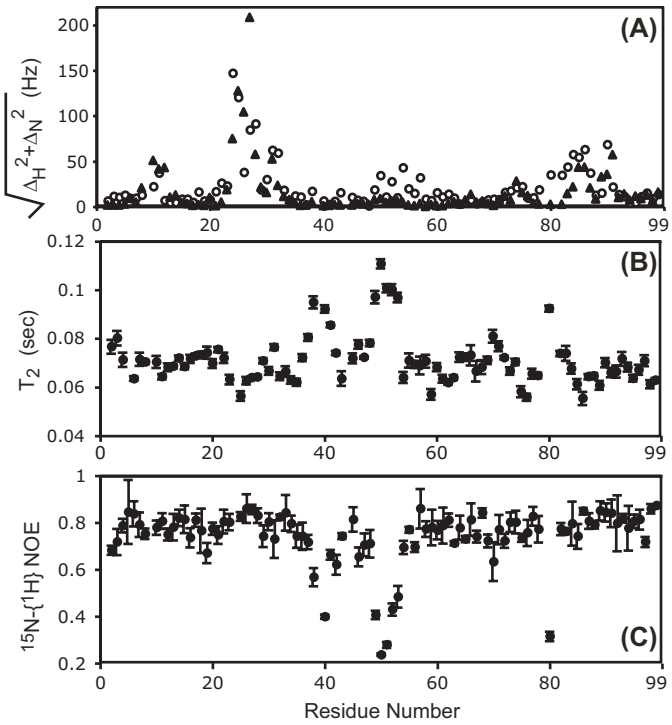

FIGURE 7. *A*, differences in the backbone amide chemical shifts of the dimer (PR *versus* PR_{D25N}, *open circles*) and the monomer (PR_{T26A} *versus* $PR_{D25N/T26A}$, *solid triangles*) with or without the D25N mutation. Δ_H and Δ_N are the differences in chemical shifts (in hertz) for the individual ^{1}H and ^{15}N atoms, respectively, in the presence and absence of the D25N mutation (plotted as the square root of the sums of their squares). The transverse relaxation times, T_2, and ^{15}N-{^{1}H} NOE values for PR_{D25N} are shown in *B* and *C*, respectively.

hydrolyzable substrate analogue, and only two crystal structures of the uninhibited wild-type mature protease have been reported so far. Similarly, we were unable to obtain crystals of free PR_{D25N}. Thus, NMR was used to examine the conformation of the PR_{D25N} dimer in the absence of a bound inhibitor. Furthermore, information derived from NMR techniques about protein dynamics in solution is complementary to the static information provided by the crystal structures. Fig. 7*A* shows a comparison of the backbone chemical shifts of PR_{D25N} with those of PR (*open circles*). Most significant differences were observed in the active site region close to the site of the mutation, and these presumably result from the change in the chemical environment caused by the D25N mutation, and not from conformational changes. The flap region (residues 47–53) and the region spanning residues 80–90 that includes the P1-loop (residues 79–83) also exhibit differences in chemical shifts in locations far from the site of mutation.

These observed differences in chemical shifts are not directly correlated with the difference in the K_d for dimer dissociation of PR and PR_{D25N}, because the chemical shift comparison does not show significant differences in the terminal β-sheet interface region. Instead, the chemical shift differences map to the upper half of the protease, *i.e.* above the active site (*cf.* Fig. 5). Protease constructs containing the T26A mutation exhibit high dimer dissociation constants ($K_d > 0.5$ mM (10)), and give NMR spectra characteristic of a stable monomer fold. Thus, chemical shift differences between PR and PR_{D25N} dimers (*open circles*, Fig. 7*A*) were compared with the corresponding differences between PR_{T26A} and $PR_{D25N/T26A}$ monomers (*solid triangles*) to determine whether the observed differences were dependent on the dimeric state of the protein. For the PR_{T26A} and $PR_{D25N/T26A}$ monomers, no chemical-shift differences were found in the flap region, and the chemical-shift differences in the P1 loop were smaller than those between the PR and PR_{D25N} dimers. Thus, the D25N mutation induces significant differences in the chemical-shift environments in the flap region and P1-loop region in the dimer, but not in the monomer. This observation is reasonable, because the side chain of residue 25 forms part of the dimer interface but is completely exposed to the solvent in the monomer. However, despite its location at the monomer surface, the D25N mutation significantly decreases the stability of the monomer fold, as shown by the 5° decrease in the T_m for $PR_{5-95/D25N}$ as compared with PR_{5-95} (Fig. 2).

^{15}N relaxation measurements of PR_{D25N} were utilized to determine whether there were significant differences in the dynamics of PR_{D25N} relative to PR. For PR_{D25N}, the transverse relaxation times, T_2 (Fig. 7*B*) and ^{15}N-{^{1}H} NOE values (Fig. 7*C*) in the flap regions increase and decrease, respectively, showing almost opposing symmetric profiles. These observations indicate that the flap regions in PR_{D25N} undergo a significant internal motion on the sub-nanosecond time scale. ^{15}N relaxation studies (26) reported for an enzymatically active protease indicated that most T_2 values in the flap region did not increase significantly for this construct, whereas PR_{D25N} exhibits increased T_2 values for residues 49–53. Although T_2 experiments at various effective field strengths are essential to identify the contribution of chemical exchange, the difference in the T_2 profiles of PR_{D25N} and active protease indicates that the dynamics of the flap region in these two proteins differ. On the basis of both chemical shifts and relaxation measurements, it is likely that the structure of PR_{D25N} differs from that of PR such that the flap-to-flap interaction in the free protein is somewhat diminished. Therefore, these NMR studies invoke a model in which lack of the carboxylic acid/carboxylate anion of residues 25 in PR_{D25N} induces slight changes in the hydrophobic core of the protease through relative orientation of the P1 loop and flaps that cause the two flaps to interact less with each other in PR_{D25N} than in PR. In the present crystal structures with bound inhibitors, a number of distances between dimer-interface residues are somewhat longer in PR_{D25N} than in PR, suggestive of weaker interactions in the terminal β-sheet region, between the Asp/Asn-25 and -25′ in the presence of RPB and in the region comprising residues Asp-29, Arg-87, and Arg-8′. However, no significant differences in the crystal structures between the two proteins were observed in the flap region, possibly because of similar closing and tightening of the flaps in both structures upon inhibitor binding.

Effect of the D25N Mutation on PR Stabilization by DRV—The clinical inhibitor DRV is one of the most tightly binding inhibitors known for HIV-1 protease (38). This inhibitor has been reported to be effective against several drug resistant protease mutants that have emerged as a result of selective pressure in the presence of other, widely-used drugs. Interactions of DRV with enzymatically active, drug-resistant mutants of PR

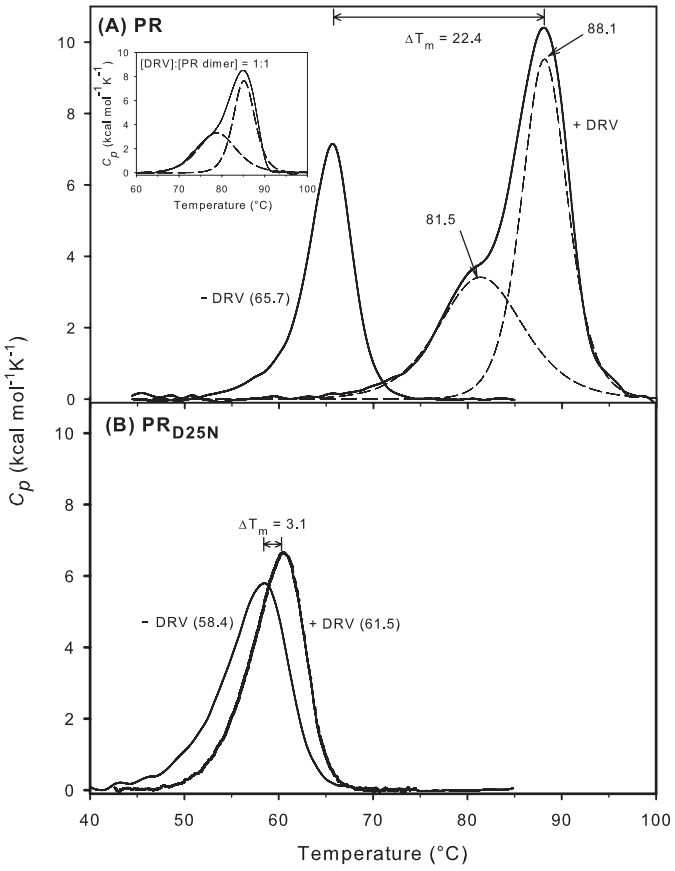

FIGURE 8. **Effect of DRV on the thermal transitions of PR (*A*) and PR_{D25N} (*B*).** Data for comparison in the absence of inhibitor are from Fig. 2; all data are normalized to protease dimer concentration. Protease dimer concentrations in the presence of DRV (28 μM total) were 14 μM. The *inset* shows a thermogram for PR·DRV (1:1) measured under the same conditions at a total DRV concentration of 13 μM, with T_m values of 78.9 and 85.2 °C. The *broken lines* show the deconvolution (using MicroCal's version of Origin software) of the two apparent transitions observed for PR in the presence of DRV.

have thus been a subject of intensive study (10).[3] Several essential residues, the most obvious of which are the catalytic Asp-25 pair, are conserved in all enzymatically active variants of the protease. Thus, comparison of inhibitor binding to active PR and inactive constructs bearing mutations at conserved residues allows assessment of the contribution made by these conserved residues to inhibitor binding. This approach is thus complementary to mapping the interactions of these inhibitors with drug-resistant PR variants in which non-conserved residues are mutated.

On the basis of our observations with RPB, we had anticipated that DRV would likely have a much greater effect on the stability of the folded PR dimer than that produced by the less tightly bound RPB. The effect of a ~2-fold molar excess of DRV on the T_m of PR confirmed this expectation. At a PR:DRV ratio of 1:2 (Fig. 8*A*) the melting curve for PR·DRV exhibits a shoulder corresponding to T_m ~82 °C and a major transition at 88.1 °C, with an area ratio of ~40/60. Successive scans of the same solution showed that the unfolding of PR·DRV was not reversible under our experimental conditions. The biphasic appearance of the thermogram was independent of the scan rate at 60 and 90 °C/h, with both T_m values slightly lower (~1 °C) at the slower scan rate. Because the concentration of DRV (28 μM) far exceeds that required for saturation of the enzyme (K_L = 4.5 pM) (38), the biphasic transition cannot be ascribed to an increase in the saturation level of the remaining enzyme and consequent increase in its T_m as the inhibitor-bound enzyme unfolds and releases free inhibitor into solution (43, 44). The two transitions could result either from the two orientations of DRV in the PR active site that have been observed in the crystal structure (31), or from occupancy of the reported second binding site to give a 2:1 complex of DRV:PR (45). If we assume that binding at the second site is of lower affinity than binding in the active site, we anticipated that in the presence of a DRV:PR ratio of 1:1, all of the inhibitor should be bound at the active site, and no inhibitor would remain to form the 2:1 complex; thus the shoulder should be absent or markedly diminished if binding at a second site were responsible for the two transitions observed at the 2:1 ratio of DRV to PR. A DSC scan in the presence of ~1 mol DRV per mol of PR (*inset*, Fig. 8) exhibited a slight decrease in the T_m for both transitions, as expected (44), because of the lower concentration of DRV; however, both transitions (T_m ~ 79 and 85.2 °C) were still present in essentially the same proportion (43/56) as observed with the 2:1 inhibitor ratio. This result is most consistent with the conclusion that these two transitions are likely to be related to the two orientations of DRV in the active site.

In remarkable contrast to PR, however, the T_m for PR_{D25N} in the presence of the same ~2-fold molar excess of DRV was minimally affected (Fig. 8*B*) and suggests that DRV binds only very weakly to PR_{D25N}. The ΔT_m of 3.1 °C induced by DRV is even smaller than that observed with RPB (6.2 °C, *cf.* Fig. 2*B*). Weak binding of DRV to PR_{D25N} was confirmed by ITC (Fig. 9), which gave a K_L of 3.2 μM at pH 5 and 28 °C, a value roughly 10-fold greater than the corresponding K_L of ~0.3 μM for PR_{D25N}·RPB and almost 6 orders of magnitude greater than K_L for PR·DRV (38). Unlike RPB, the dramatic difference in binding affinity of DRV to PR relative to PR_{D25N} results from large favorable differences in both entropy and enthalpy (Table 1). These large differences in binding affinity and energetics are accompanied by only minor effects on the protein conformation surrounding the active site. We conclude that a major contribution to the tight binding of DRV is made by specific interactions mediated by the catalytic Asp residues. Other tight binding inhibitors contain a similar central motif consisting of a hydroxyl group that can hydrogen bond to the catalytic Asp-25, flanked by two hydrophobic moieties at the P1 and P1′ positions (indicated by the *black arrow* in Figs. 5*A* and 6*A* (42, 46)). These central hydroxyl-containing motifs generally align well with each other upon superimposition of crystal structures of their PR complexes. Thus we predict that the strength of the interaction with the catalytic Asp pair of PR and its contribution to the overall binding affinity should be relatively invariant for these inhibitors.

Concluding Remarks—The D25N mutation lowers the K_d and T_m of PR by >100-fold and by 7.3 °C, respectively, whereas completely abolishing the dimer interface in the mutant PR_{5-95} lowers the T_m by 10 °C. NMR studies of the inhibitor-free PR and PR_{D25N} suggest that the principal difference between these

[3] HIV Drug Resistance Database: hivdb.stanford.edu/index.html.

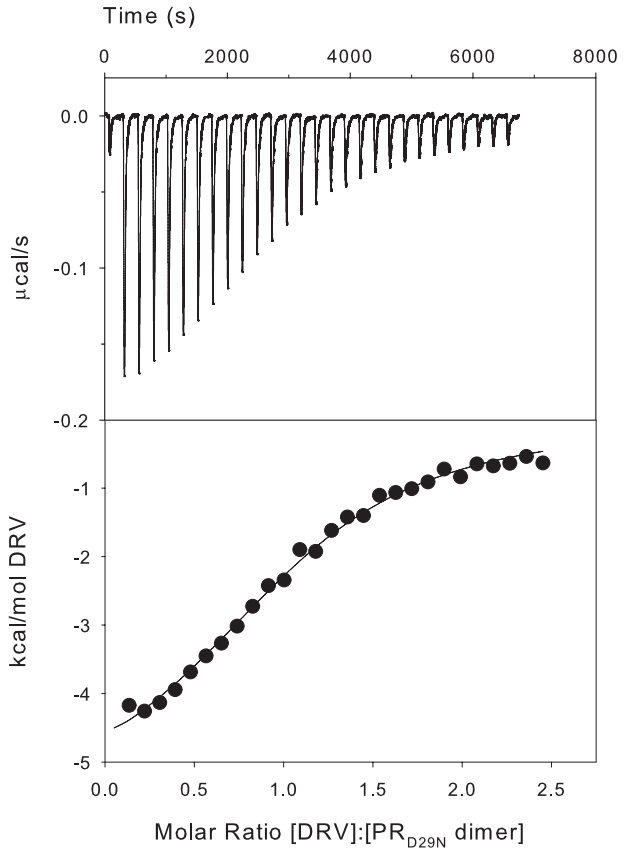

FIGURE 9. **ITC of PR_{D25N} with DRV in 50 mM sodium acetate buffer, pH 5, at 28 °C.** *Upper panel*, thermal changes on addition of 3- (first injection) and 5-μl (subsequent injections) aliquots of 266 μM DRV solution to 11 μM PR_{D25N} dimer in the calorimetric cell (~1.43 ml). Curve fitting of the integrated data (*lower panel*) gave a dissociation constant, K_L, for DRV of ~3.2 μM (reciprocal of $K_a = 3.17 \times 10^5\ M^{-1}$; see Table 1).

two proteins resides in the P1 loop and flap regions, which are known to be relatively mobile. These results indicate that the active site Asp residues make a large and specific contribution to the stabilization of the monomer fold and dimerization.

The D25N mutation produces a striking change in the interaction between the protease and the clinical inhibitor DRV, as demonstrated by the a minimal increase (3 °C) in the T_m of PR_{D25N}·DRV as compared with a 22° increase in the T_m of PR·DRV under the same conditions, as well as the ~10^6-fold less favorable binding constant for DRV to PR_{D25N} as compared with PR. However, the high resolution structural data described here indicate only subtle differences between the active site and dimer-interface geometry of PR and PR_{D25N} when bound to inhibitors. Thus, the critical role of Asp-25 in maintaining the dimer stability when bound to DRV appears not to be primarily steric in origin and most likely is related to an interaction of the OH of DRV with a carboxyl group that is lost on substitution with an amide.

The use of DSC and ITC to screen potential inhibitors with PR_{D25N} or other constructs mutated at residues required for enzymatic activity is complementary to current approaches that utilize catalytically active, drug-resistant mutants. We suggest that this approach will provide a useful and hitherto unexploited tool to identify leads for inhibitors that specifically target highly conserved, catalytically and/or structurally critical residues, and are thus most likely to retain pharmacological activity against drug-resistant strains. Furthermore, the finding that D25N mutation destabilizes the dimer with a >100-fold increase in K_d may prove to be useful in screening lead compounds that block dimerization under conditions that permit observation by physical methods of the dimer-monomer equilibrium at a more convenient protein concentrations, *i.e.* well above the low nanomolar range exhibited by PR.

Acknowledgments—We thank D. A. Torchia, A. Y. Kovalevsky, and R. W. Harrison for helpful discussions, F. Delaglio and D. Garrett for data processing software, A. Aniana for expert technical assistance, Y.-F. Wang for help with supplemental Fig. S2, and A. Ghosh for generously providing DRV prior to its availability from the NIH AIDS research and reference reagent program, Division of AIDS, NIAID, NIH (Reagent 11447 from Tibotec Pharmaceuticals).

REFERENCES

1. Oroszlan, S., and Luftig, R. B. (1990) *Curr. Top. Microbiol. Immunol.* **157,** 153–185
2. Kohl, N. E., Emini, E. A., Schleif, W. A., Davis, L. J., Heimbach, J. C., Dixon, R. A., Scolnick, E. M., and Sigal, I. S. (1988) *Proc. Natl. Acad. Sci. U. S. A.* **85,** 4686–4690
3. Louis, J. M., Weber, I. T., Tozser, J., Clore, G. M., and Gronenborn, A. M. (2000) *Adv. Pharmacol.* **49,** 111–146
4. Kaplan, A. H., Manchester, M., and Swanstrom, R. (1994) *J. Virol.* **68,** 6782–6786
5. Kaplan, A. H., Zack, J. A., Knigge, M., Paul, D. A., Kempf, D. J., Norbeck, D. W., and Swanstrom, R. (1993) *J. Virol.* **67,** 4050–4055
6. Karacostas, V., Wolffe, E. J., Nagashima, K., Gonda, M. A., and Moss, B. (1993) *Virology* **193,** 661–671
7. Krausslich, H. G. (1991) *Proc. Natl. Acad. Sci. U. S. A.* **88,** 3213–3217
8. Erickson, J. W., and Burt, S. K. (1996) *Annu. Rev. Pharmacol. Toxicol.* **36,** 545–571
9. Weber, I. T., Kovalevsky, A. Y., and Harrison, R. W. (2007) *Frontiers Drug Design Discov.* **3,** 45–62
10. Louis, J. M., Ishima, R., Torchia, D. A., and Weber, I. T. (2007) *Adv. Pharmacol.* **55,** 261–298
11. Rodriguez-Barrios, F., and Gago, F. (2004) *Curr. Top. Med. Chem.* **4,** 991–1007
12. Temesgen, Z., Warnke, D., and Kasten, M. J. (2006) *Expert. Opin. Pharmacother.* **7,** 1541–1554
13. Pearl, L. H., and Taylor, W. R. (1987) *Nature* **329,** 351–354
14. Wlodawer, A., and Erickson, J. (1993) *Annu. Rev. Biochem.* **62,** 543–585
15. Rodriguez, E. J., Angeles, T. S., and Meek, T. D. (1993) *Biochemistry* **32,** 12380–12385
16. Wlodawer, A., Miller, M., Jaskolski, M., Sathyanarayana, B. K., Baldwin, E., Weber, I. T., Selk, L. M., Clawson, L., Schneider, J., and Kent, S. B. (1989) *Science* **245,** 616–621
17. Babe, L. M., Rose, J., and Craik, C. S. (1995) *Proc. Natl. Acad. Sci. U. S. A.* **92,** 10069–10073
18. Prabu-Jeyabalan, M., Nalivaika, E., and Schiffer, C. A. (2000) *J. Mol. Biol.* **301,** 1207–1220
19. Sluis-Cremer, N., and Tachedjian, G. (2002) *Eur. J. Biochem.* **269,** 5103–5111
20. Weber, I. T. (1990) *J. Biol. Chem.* **265,** 10492–10496
21. Katoh, E., Louis, J. M., Yamazaki, T., Gronenborn, A. M., Torchia, D. A., and Ishima, R. (2003) *Protein Sci.* **12,** 1376–1385
22. Louis, J. M., Clore, G. M., and Gronenborn, A. M. (1999) *Nat. Struct. Biol.* **6,** 868–875
23. Ishima, R., Torchia, D. A., and Louis, J. M. (2007) *J. Biol. Chem.* **282,** 17190–17199
24. Ishima, R., Torchia, D. A., Lynch, S. M., Gronenborn, A. M., and Louis, J. M. (2003) *J. Biol. Chem.* **278,** 43311–43319

25. Ishima, R., Louis, J. M., and Torchia, D. A. (2001) *J. Mol. Biol.* **305,** 515–521
26. Freedberg, D. I., Ishima, R., Jacob, J., Wang, Y. X., Kustanovich, I., Louis, J. M., and Torchia, D. A. (2002) *Protein Sci.* **11,** 221–232
27. Otwinowski, Z., and Minor, W. (1997) *Methods Enzymol.* **276,** 307–326
28. Navaza, J. (1994) *Acta Crystallogr. Sect. D Biol. Crystallogr.* **50,** 157–163
29. Sheldrick, G. M., and Schneider, T. R. (1997) *Methods Enzymol.* **277,** 319–343
30. Jones, T. A., Zou, J. Y., Cowan, S. W., and Kjeldgaard, M. (1991) *Acta Crystallogr. Sect. A* **47,** 110–119
31. Tie, Y., Boross, P. I., Wang, Y. F., Gaddis, L., Hussain, A. K., Leshchenko, S., Ghosh, A. K., Louis, J. M., Harrison, R. W., and Weber, I. T. (2004) *J. Mol. Biol.* **338,** 341–352
32. Ishima, R., Ghirlando, R., Tozser, J., Gronenborn, A. M., Torchia, D. A., and Louis, J. M. (2001) *J. Biol. Chem.* **276,** 49110–49116
33. Xie, D., Gulnik, S., Gustchina, E., Yu, B., Shao, W., Qoronfleh, W., Nathan, A., and Erickson, J. W. (1999) *Protein Sci.* **8,** 1702–1707
34. Beissinger, M., Paulus, C., Bayer, P., Wolf, H., Rosch, P., and Wagner, R. (1996) *Eur. J. Biochem.* **237,** 383–392
35. Wondrak, E. M., and Louis, J. M. (1996) *Biochemistry* **35,** 12957–12962
36. Tie, Y., Boross, P. I., Wang, Y. F., Gaddis, L., Liu, F., Chen, X., Tozser, J., Harrison, R. W., and Weber, I. T. (2005) *FEBS J.* **272,** 5265–5277
37. Liu, F., Boross, P. I., Wang, Y. F., Tozser, J., Louis, J. M., Harrison, R. W., and Weber, I. T. (2005) *J. Mol. Biol.* **354,** 789–800
38. King, N. M., Prabu-Jeyabalan, M., Nalivaika, E. A., Wigerinck, P., de Bethune, M. P., and Schiffer, C. A. (2004) *J. Virol.* **78,** 12012–12021
39. Liu, F., Kovalevsky, A. Y., Louis, J. M., Boross, P. I., Wang, Y. F., Harrison, R. W., and Weber, I. T. (2006) *J. Mol. Biol.* **358,** 1191–1199
40. Mahalingam, B., Wang, Y. F., Boross, P. I., Tozser, J., Louis, J. M., Harrison, R. W., and Weber, I. T. (2004) *Eur. J. Biochem.* **271,** 1516–1524
41. Strisovsky, K., Tessmer, U., Langner, J., Konvalinka, J., and Krausslich, H. G. (2000) *Protein Sci.* **9,** 1631–1641
42. Klei, H. E., Kish, K., Lin, P. F., Guo, Q., Friborg, J., Rose, R. E., Zhang, Y., Goldfarb, V., Langley, D. R., Wittekind, M., and Sheriff, S. (2007) *J. Virol.* **81,** 9525–9535
43. Shrake, A., and Ross, P. D. (1992) *Biopolymers* **32,** 925–940
44. Brandts, J. F., and Lin, L. N. (1990) *Biochemistry* **29,** 6927–6940
45. Kovalevsky, A. Y., Liu, F., Leshchenko, S., Ghosh, A. K., Louis, J. M., Harrison, R. H., and Weber, I. T. (2006) *J. Mol. Biol.* **363,** 161–173
46. Stoll, V., Qin, W., Stewart, K. D., Jakob, C., Park, C., Walter, K., Simmer, R. L., Helfrich, R., Bussiere, D., Kao, J., Kempf, D., Sham, H. L., and Norbeck, D. W. (2002) *Bioorg. Med. Chem.* **10,** 2803–2806